Noname manuscript No.
(will be inserted by the editor)

Indirectly-controlled limit cycle walking of combined rimless wheel based on entrainment to active wobbling motion

Fumihiko Asano · Isao Tokuda

Received: date / Accepted: date

Abstract It has been clarified that a passive combined rimless wheel (CRW) that consists of two identical eight-legged rimless wheels can increase the walking speed either by adjusting the phase difference between the fore and rear legs or by using a passive wobbling mass that vibrates up-and-down in the body frame. Towards a further speeding-up of the CRW, this paper investigates the effect of an active wobbling mass driven by an actuator and the effect of an indirect excitation control. First, we develop the mathematical model and numerically show that the CRW generates a walking motion, which is entrained to the up-and-down motion of the active wobbling mass at frequencies higher than the natural frequency of the CRW. We discuss the gait properties mainly from the viewpoints of frequency and phase relationships. Second, we conduct verification experiments using our prototype CRW machine and describe the results.

Keywords Combined rimless wheel · Passive dynamic walking · Entrainment · Wobbling mass ·

F. Asano
School of Information Science, Japan Advanced Institute of Science and Technology
1-1 Asahidai, Nomi, Ishikawa 923-1292, Japan
Tel.: +81-761-51-1243
Fax: +81-761-51-1149
E-mail: fasano@jaist.ac.jp

I. Tokuda
Department of Mechanical Engineering, College of Science and Engineering, Ritsumeikan University
1-1-1 Nojihigashi, Kusatsu, Shiga 525-8577, Japan
E-mail: isao@fc.ritsumei.ac.jp

1 Introduction

Limit cycle walking inspired by passive-dynamic walking [1] is a favorable approach to efficient robotic legged locomotion and various types of limit cycle walkers such as biped [2][3], quadruped [4], and multilegged robots [5] have been investigated and developed. The easiest way to achieve efficient level walking is adding small torque inputs to a passive-dynamic walker and the generated walking gait in most cases converges to a stationary orbit with impulsive effects according to the inherent stability. It is empirically known that generating stable limit cycle walking is not difficult but the mechanisms necessary to achieve it remain to be elucidated. The motion of a rimless wheel (RW) is specified as a simple 1-DOF dynamics and therefore is a good example for investigating the properties and mechanisms of a limit cycle walking such as stability [1][6][7], efficiency and gait symmetry [8]. The authors started the study of a combined rimless wheel (CRW) as the simplest multilegged passive-dynamic walker and have investigated what advantages are produced by the combined body structure. So far, we clarified the following properties appearing in the generated gait.

We first showed that the walking speed of the passive CRW can be increased by adjusting the phase difference between the fore and rear legs through numerical and experimental investigations [9]. The results showed that the walking speed becomes maximum as the phase difference approaches to half of the hip angle. The speeding-up mechanism can be explained as resulting from flattening of the trajectory of the whole center of mass (CoM). After that, we added a passive wobbling mass that moves up-and-down in the body frame for the purpose of flattening the CoM trajectory even when the fore-rear phase difference is zero [10]. Through gait analysis, we clarified that a passive wobbling mass also increases the walking speed by exhibiting anti-phase oscillations. In addition, some interesting nonlinear phenomena such as hysteresis and sensitive dependence on initial conditions were also observed. Some related results were reported in [4][11][12][13].

Limitation of the passive wobbling mass is that it can exhibit anti-phase oscillations only when its natural frequency is lower than that of the CRW. Increase in the natural frequency results in an in-phase synchronization, which slows down the walking. A modified mechanism is needed to further speed up the walking.

Based on these observations, in this paper, we investigate the effect of a wobbling mass that actively moves up-and-down in the body frame. The active wobbling mass can generate anti-phase oscillations even when its natural frequency is much higher than that of the CRW. Here, the walking speed is increased not only by the flattening effect of the CoM trajectory but also by the fast oscillations of the active wobbling mass. First, we perform numerical simulations to clarify the fundamental gait properties and discuss how the passive-dynamics and the inherent rhythmical movement of a CRW are changed according to the active wobbling frequency, especially from the per-

spective of frequency difference. Second, we conduct verification experiments using a prototype CRW machine with three different wobbling masses.

This paper is organized as follows. In Section 2, a mathematical model is developed for a CRW with an active wobbling mass and its reduction to a model of low degrees of freedom is described. In Section 3, typical walking gaits with the effect of wobbling motion are observed. In Section 4, gait analysis is conducted and the possibility of speeding-up by entraining the CRW to the wobbling motion at high frequencies is numerically demonstrated. In Section 5, the validity of the numerical results are experimentally-verified using a prototype CRW machine. Finally, Section 6 concludes this paper and describes future research directions.

2 Modeling and control

2.1 Equations of motion and its reduction

Fig. 1 shows the model of a passive CRW with an active wobbling mass. This walker consists of two identical eight-legged RWs, a body frame, and the active wobbling mass in the body. The model is based on the following assumptions.

- The two RWs perfectly synchronize with no phase difference between the fore and rear RWs. Under this condition, our quadruped system can be considered as a single RW. They always contact with the ground without slipping.
- The two RWs are connected to the body frame without incorporating joint friction. They rotate passively.

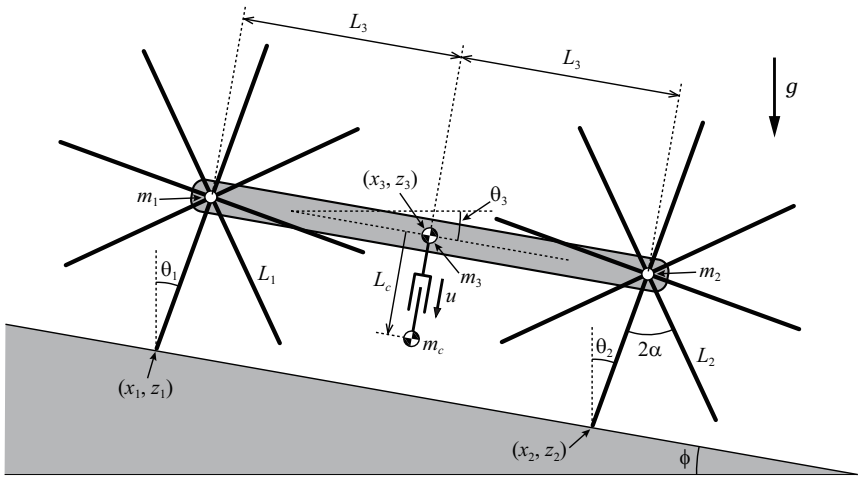

Fig. 1 Model of combined rimless wheel with active wobbling mass

– The configuration of the RW is symmetric and all the relative angles between any two adjacent leg frames are $2\alpha = 45$ [deg].

Let $\boldsymbol{q} = \begin{bmatrix} x_1 & z_1 & \theta_1 & x_2 & z_2 & \theta_2 & x_3 & z_3 & \theta_3 & L_c \end{bmatrix}^{\mathrm{T}}$ be the generalized coordinate vector. As indicated in Fig. 1, (x_1, z_1) and (x_2, z_2) are the end positions of the rear and fore RWs' stance legs. (x_3, z_3) is the CoM position of the body frame. θ_1 and θ_2 are the angular positions of the rear and fore RWs with respect to the vertical. θ_3 is the angular position of the body frame with respect to the horizontal. L_c is the length of the active wobbling mass attached quartering to the body frame.

The other parameters are defined as follows. $m_1 = m_2$ [kg] is the mass of each RW. m_3 [kg] is the mass of the body frame. m_c [kg] is the mass of the wobbling mass. $L_1 = L_2 = L$ [m] are the radius or the leg length of each RW. $2L_3$ [m] is the length of the body frame. The CoM is located at the central position.

The equation of motion then becomes

$$\boldsymbol{M}(\boldsymbol{q})\ddot{\boldsymbol{q}} + \boldsymbol{h}(\boldsymbol{q}, \dot{\boldsymbol{q}}) = \boldsymbol{S}u + \boldsymbol{J}(\boldsymbol{q})^{\mathrm{T}}\boldsymbol{\lambda}, \tag{1}$$

$$\boldsymbol{J}(\boldsymbol{q})\dot{\boldsymbol{q}} = \boldsymbol{0}_{8\times 1}, \tag{2}$$

where $\boldsymbol{S} = \begin{bmatrix} \boldsymbol{0}_{1\times 9} & 1 \end{bmatrix}^{\mathrm{T}}$ and u [N] is the actuator force to control the wobbling mass. The time-derivative of Eq. (2) becomes

$$\boldsymbol{J}(\boldsymbol{q})\ddot{\boldsymbol{q}} + \dot{\boldsymbol{J}}\left(\boldsymbol{q}, \dot{\boldsymbol{q}}\right)\dot{\boldsymbol{q}} = \boldsymbol{0}_{8\times 1}. \tag{3}$$

Then we can solve the system of equations (1) and (3) for the holonomic constraint force term, $\boldsymbol{\lambda}$, as follows.

$$\boldsymbol{\lambda} = -\boldsymbol{X}(\boldsymbol{q})^{-1}\left(\boldsymbol{J}(\boldsymbol{q})\boldsymbol{M}(\boldsymbol{q})^{-1}\left(\boldsymbol{S}u - \boldsymbol{h}(\boldsymbol{q}, \dot{\boldsymbol{q}})\right) + \dot{\boldsymbol{J}}(\boldsymbol{q}, \dot{\boldsymbol{q}})\dot{\boldsymbol{q}}\right) \tag{4}$$

$$\boldsymbol{X}(\boldsymbol{q}) := \boldsymbol{J}(\boldsymbol{q})\boldsymbol{M}(\boldsymbol{q})^{-1}\boldsymbol{J}(\boldsymbol{q})^{\mathrm{T}} \tag{5}$$

By substituting Eq. (4) into Eq. (1) and arranging it, we get

$$\boldsymbol{M}(\boldsymbol{q})\ddot{\boldsymbol{q}} = \boldsymbol{Y}(\boldsymbol{q})\left(\boldsymbol{S}u - \boldsymbol{h}(\boldsymbol{q}, \dot{\boldsymbol{q}})\right) - \boldsymbol{J}(\boldsymbol{q})^{\mathrm{T}}\boldsymbol{X}(\boldsymbol{q})^{-1}\dot{\boldsymbol{J}}(\boldsymbol{q}, \dot{\boldsymbol{q}})\dot{\boldsymbol{q}}, \tag{6}$$

$$\boldsymbol{Y}(\boldsymbol{q}) := \boldsymbol{I}_{10} - \boldsymbol{J}(\boldsymbol{q})^{\mathrm{T}}\boldsymbol{X}(\boldsymbol{q})^{-1}\boldsymbol{J}(\boldsymbol{q})\boldsymbol{M}(\boldsymbol{q})^{-1}. \tag{7}$$

In the case that the fore and rear legs perfectly synchronize with each other with a zero phase difference, the velocity vector has the form

$$\dot{\boldsymbol{q}} = \begin{bmatrix} \boldsymbol{0}_{2\times 1} \\ \dot{\theta}_1 \\ \boldsymbol{0}_{2\times 1} \\ \dot{\theta}_1 \\ L\dot{\theta}_1\cos\theta_1 \\ -L\dot{\theta}_1\sin\theta_1 \\ 0 \\ \dot{L}_c \end{bmatrix}. \tag{8}$$

By using this relation, we can derive the acceleration vector as follows.

$$\ddot{\boldsymbol{q}} = \begin{bmatrix} \mathbf{0}_{2\times 1} \\ N_{\theta_1}/D_{\theta_1} \\ \mathbf{0}_{2\times 1} \\ N_{\theta_1}/D_{\theta_1} \\ N_{x_3}/D_{x_3} \\ N_{z_3}/D_{z_3} \\ 0 \\ N_{L_c}/D_{L_c} \end{bmatrix} \tag{9}$$

All the numerators and denominators are functions only of the rear RW's dynamics, θ_1 and $\dot{\theta}_1$, and the control force, u. The dynamics of the body frame is not related to the generated motion and all the necessary variables for numerical integral are only θ_1, L_c, and their time-derivatives. Therefore we can reduce the 10-DOF redundant system to the following 2-DOF one.

$$\ddot{\theta}_1 = \frac{N_{\theta_1}}{D_{\theta_1}}, \quad \ddot{L}_c = \frac{N_{L_c}}{D_{L_c}} \tag{10}$$

The terms in Eq. (10) are detailed as follows.

$$\begin{aligned} N_{\theta_1} &= (2m_w + m_c)g\sin\theta_1 - m_c g\sin(\theta_1 - 2\theta_3) + m_c L\dot{\theta}_1^2 \sin(2(\theta_1 - \theta_3)) \\ &\quad -2\sin(\theta_1 - \theta_3)u \\ D_{\theta_1} &= 2L(m_w + m_c\cos^2(\theta_1 - \theta_3)) \\ N_{L_c} &= (m_w + m_c)\left(u + m_c\left(g\cos\theta_1 - L\dot{\theta}_1^2\right)\cos(\theta_1 - \theta_3)\right) \\ D_{L_c} &= m_c(m_w + m_c\cos^2(\theta_1 - \theta_3)) \end{aligned}$$

Here, $m_w := 2m_1 + m_3$ [kg] is the total mass of the CRW except the wobbling mass. Note that θ_3 is equal to the slope angle, ϕ [rad], and is constant. The vertical ground reaction force, λ_2, is also derived as follows.

$$\begin{aligned} \lambda_2 &= -\frac{N_{\lambda_2}}{D_{\lambda_2}} \\ N_{\lambda_2} &= \cos\theta_1\left(m_w(L\dot{\theta}_1^2 - g\cos\theta_1) + \cos(\theta_1 - \theta_3)u\right) \\ &\quad \times ((m_w + m_c)L_3 - m_c L_c\tan(\theta_1 - \theta_3)) \\ D_{\lambda_2} &= 2L_3\left(m_w + m_c\cos^2(\theta_1 - \theta_3)\right) \end{aligned}$$

Then we can check the condition for unilateral constraint by observing λ_2. A stable walking is achieved when λ_2 is always positive.

2.2 Collision equations and its analysis

In this paper, we assume that the rear legs of both RWs at impact leaves the ground immediately after landing of the fore legs according to the inelastic collision model which is specified as

$$\boldsymbol{M}(\boldsymbol{q})\dot{\boldsymbol{q}}^{+} = \boldsymbol{M}(\boldsymbol{q})\dot{\boldsymbol{q}}^{-} + \boldsymbol{J}_I(\boldsymbol{q})^{\mathrm{T}}\boldsymbol{\lambda}_I, \tag{11}$$

$$\boldsymbol{J}_I(\boldsymbol{q})\dot{\boldsymbol{q}}^{+} = \boldsymbol{0}_{8\times 1}. \tag{12}$$

Note that $\boldsymbol{q}^{+} = \boldsymbol{q}^{-} = \boldsymbol{q}$ holds in these equations. $\boldsymbol{J}_I(\boldsymbol{q}) \in \mathbb{R}^{8\times 10}$ and its elements are detailed as follows.

$$\boldsymbol{J}_I(\boldsymbol{q}) = \begin{bmatrix}
1 & 0 & J_{I(13)} & 0 & 0 & 0 & 0 & 0 & 0 & 0 \\
0 & 1 & J_{I(23)} & 0 & 0 & 0 & 0 & 0 & 0 & 0 \\
0 & 0 & 0 & 1 & 0 & J_{I(36)} & 0 & 0 & 0 & 0 \\
0 & 0 & 0 & 0 & 1 & J_{I(46)} & 0 & 0 & 0 & 0 \\
1 & 0 & L\cos\theta_1^{-} & 0 & 0 & 0 & -1 & 0 & -L_3\sin\theta_3^{-} & 0 \\
0 & 1 & -L\sin\theta_1^{-} & 0 & 0 & 0 & 0 & -1 & -L_3\cos\theta_3^{-} & 0 \\
0 & 0 & 0 & 1 & 0 & L\cos\theta_2^{-} & -1 & 0 & L_3\sin\theta_3^{-} & 0 \\
0 & 0 & 0 & 0 & 1 & -L\sin\theta_2^{-} & 0 & -1 & L_3\cos\theta_3^{-} & 0
\end{bmatrix}$$

$$J_{I(13)} = L\left(\cos\theta_1^{-} - \cos\left(\theta_1^{-} - 2\alpha\right)\right)$$

$$J_{I(23)} = -L\left(\sin\theta_1^{-} - \sin\left(\theta_1^{-} - 2\alpha\right)\right)$$

$$J_{I(36)} = L\left(\cos\theta_2^{-} - \cos\left(\theta_2^{-} - 2\alpha\right)\right)$$

$$J_{I(46)} = -L\left(\sin\theta_2^{-} - \sin\left(\theta_2^{-} - 2\alpha\right)\right)$$

By solving Eqs. (11) and (12) for $\dot{\boldsymbol{q}}^{+}$, we can obtain the velocity vector immediately after impact as follows.

$$\dot{\boldsymbol{q}}^{+} = \left(\boldsymbol{I}_{10} - \boldsymbol{M}(\boldsymbol{q})^{-1}\boldsymbol{J}_I(\boldsymbol{q})^{\mathrm{T}}\left(\boldsymbol{J}_I(\boldsymbol{q})\boldsymbol{M}(\boldsymbol{q})^{-1}\boldsymbol{J}_I(\boldsymbol{q})^{\mathrm{T}}\right)^{-1}\boldsymbol{J}_I(\boldsymbol{q})\right)\dot{\boldsymbol{q}}^{-} \tag{13}$$

Elements of $\dot{\boldsymbol{q}}^{+}$ are detailed as follows. Note, however, that the relations of $\theta_1^{-} = \phi + \alpha$ and $\theta_3^{-} = \phi$ were considered.

$$\dot{x}_1^{+} = \dot{x}_2^{+} = \frac{2L\sin\alpha\sin\phi\left(m_w\cos(2\alpha) + m_c\cos^2\alpha\right)}{m_w + m_c\cos^2\alpha}\dot{\theta}_1^{-} \tag{14}$$

$$\dot{z}_1^{+} = \dot{z}_2^{+} = \frac{2L\sin\alpha\cos\phi\left(m_w\cos(2\alpha) + m_c\cos^2\alpha\right)}{m_w + m_c\cos^2\alpha}\dot{\theta}_1^{-} \tag{15}$$

$$\dot{\theta}_1^{+} = \dot{\theta}_2^{+} = \frac{m_w\cos(2\alpha) + m_c\cos^2\alpha}{m_w + m_c\cos^2\alpha}\dot{\theta}_1^{-} \tag{16}$$

$$\dot{x}_3^{+} = \frac{L\cos(\alpha-\phi)\left(m_w\cos(2\alpha) + m_c\cos^2\alpha\right)}{m_w + m_c\cos^2\alpha}\dot{\theta}_1^{-} \tag{17}$$

$$\dot{z}_3^{+} = \frac{L\sin(\alpha-\phi)\left(m_w\cos(2\alpha) + m_c\cos^2\alpha\right)}{m_w + m_c\cos^2\alpha}\dot{\theta}_1^{-} \tag{18}$$

$$\dot{\theta}_3^{+} = 0 \tag{19}$$

$$\dot{L}_c^{+} = \dot{L}_c^{-} + \frac{(m_w + m_c)L\sin(2\alpha)\cos\alpha}{m_w + m_c\cos^2\alpha}\dot{\theta}_1^{-} \tag{20}$$

From the above equations, we can understand that all the velocities immediately after impact can be specified as functions only of $\dot{\theta}_1^-$ and $\dot{L}_c^-$. The necessary state variables at impact therefore are only θ_1 and L_c as in the equation of motion.

After calculating $\dot{\theta}_1^+$ and $\dot{L}_c^+$, we should reset θ_1 and L_c as follows.

$$\theta_1^+ = \theta_1^- - 2\alpha = \phi - \alpha, \quad L_c^+ = L_c^- \tag{21}$$

By performing the calculations of Eqs. (16), (20) and (21), stance-leg exchange can be completed.

Here, let us revisit the collision equation of Eq. (16). This can be arranged to

$$\dot{\theta}_1^+ = R(\alpha, \beta)\dot{\theta}_1^-, \quad R(\alpha, \beta) = \frac{\cos(2\alpha) + \beta\cos^2\alpha}{1 + \beta\cos^2\alpha}, \tag{22}$$

where $\beta := m_c/m_w$ [-] is the ratio of the wobbling mass to that of the CRW. Note that the value of $R(\alpha, \beta)$ is larger than 0 and is smaller than 1 and that decrease in angular velocity can be suppressed as $R(\alpha, \beta)$ becomes larger. $R(\alpha, \beta) = 1$ implies that there is no rotational energy loss at impact, and this is achieved by $\alpha \to 0$ or $\beta \to \infty$. In addition, $R(\alpha, 0) = \cos(2\alpha)$ holds and this is identical to the case of a single RW without inertia moment. The partial derivatives of $R(\alpha, \beta)$ with respect to α and β respectively become

$$\frac{\partial R(\alpha, \beta)}{\partial \alpha} = \frac{-2(1+\beta)\sin(2\alpha)}{(1 + \beta\cos^2\alpha)^2} < 0,$$
$$\frac{\partial R(\alpha, \beta)}{\partial \beta} = \frac{\sin^2(2\alpha)}{2(1 + \beta\cos^2\alpha)^2} > 0.$$

From these equations, we can understand that rotational energy loss at impact monotonically decreases as α decreases or as β increases. Fig. 2 plots the value of $R(\alpha, \beta)$ for $0 \leq \alpha \leq \pi/4$ [rad] and $10^{-3} \leq \beta \leq 10^3$ [-]. Note that β is represented in a logarithmic plot. We can confirm the property of $R(\alpha, \beta)$.

Small α implies that the RW motion approaches to a rolling motion without energy loss. Large β, i.e. a heavy wobbling mass, makes a kinetic energy loss at impact smaller. This is because, without going into detail, the most kinetic energy in the wobbling mass can be stored in the direction of the wobbling motion.

On the other hand, we can understand that, from Eq. (20), $\dot{L}_c^+ > \dot{L}_c^-$ always holds because $\dot{\theta}_1^-$ is positive. This will be confirmed through numerical simulations in the next section.

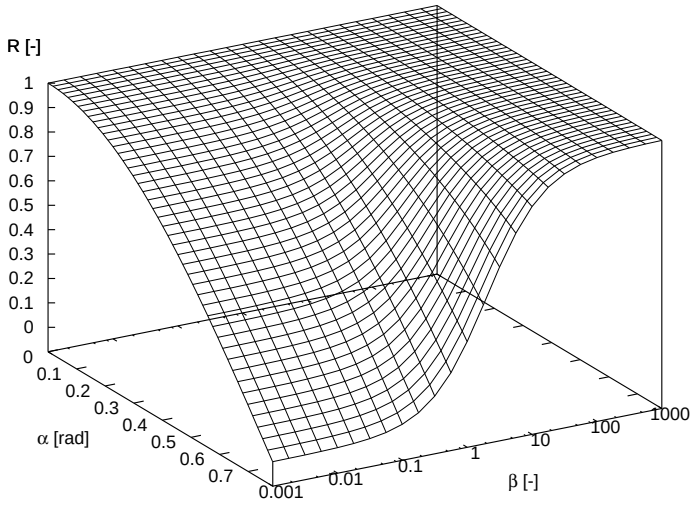

Fig. 2 $R(\alpha, \beta)$ with respect to α and β

2.3 Trajectory tracking control

Let L_c [m] be the control output. This can be written as $L_c = \boldsymbol{S}^{\mathrm{T}}\boldsymbol{q}$ and its second-order derivative with respect to time becomes

$$\begin{aligned}\ddot{L}_c &= \boldsymbol{S}^{\mathrm{T}}\ddot{\boldsymbol{q}} \\ &= \boldsymbol{M}(\boldsymbol{q})^{-1}\boldsymbol{Y}(\boldsymbol{q})\left(\boldsymbol{S}u - \boldsymbol{h}(\boldsymbol{q}, \dot{\boldsymbol{q}})\right) + \boldsymbol{M}(\boldsymbol{q})^{-1}\boldsymbol{J}(\boldsymbol{q})^{\mathrm{T}}\boldsymbol{X}(\boldsymbol{q})^{-1}\dot{\boldsymbol{J}}(\boldsymbol{q}, \dot{\boldsymbol{q}})\dot{\boldsymbol{q}} \\ &= A(\theta_1)u + B(\theta_1, \dot{\theta}_1) \end{aligned} \tag{23}$$

where

$$A(\theta_1) = \frac{m_w + m_c}{m_c(m_w + m_c\cos^2(\theta_1 - \theta_3))},$$

$$B(\theta_1, \dot{\theta}_1) = \frac{(m_w + m_c)\left(g\cos\theta_1 - L\dot{\theta}_1^2\right)\cos(\theta_1 - \theta_3)}{m_w + m_c\cos^2(\theta_1 - \theta_3)}.$$

Then we can consider the control input for achieving $L_c \to L_d(t)$ as

$$u = A(\theta_1)^{-1}\left(v - B(\theta_1, \dot{\theta}_1)\right), \tag{24}$$

$$v = \ddot{L}_d(t) + K_D\left(\dot{L}_d(t) - \dot{L}_c\right) + K_P\left(L_d(t) - L_c\right), \tag{25}$$

where K_P and K_D are PD gains and are positive constants. $L_d(t)$ is the desired-time trajectory of L_c and is given as

$$L_d(t) = A_m \sin\left(2\pi f_c t\right). \tag{26}$$

Here, f_c [Hz] is the desired frequency of the wobbling mass and A_m [m] is the desired amplitude of the pumping motion.

3 Typical walking gaits

First, we perform numerical simulations using the derived equations to observe typical walking gaits. The physical parameters are chosen as listed in Table 1. These parameters are close to those of the experimental machine introduced in Section 5. The initial conditions are also chosen as follows.

$$\theta_1(0) = \phi - \alpha, \quad L_c(0) = 0, \quad \dot{\theta}_1(0) = 4.0, \quad \dot{L}_c(0) = 2\pi f_c A_m \tag{27}$$

The walker therefore starts walking from the impact posture with a sufficient initial angular velocity for overcoming the potential barrier. The initial wobbling velocity, $\dot{L}_c(0)$, is also set to be the same as the desired one, $\dot{L}_d(0) = 2\pi f_c A_m$, to avoid excessive initial control input at the beginning of walking. A large control input causes violent changes of acceleration, which may easily violate unilateral constraint condition.

Fig. 3 shows the simulation results of dynamic walking where $f_c = 1.0$ [Hz]. As described later, in this case, the wobbling motion has little effect on the dynamics of the CRW (generated gait). Fig. 3 (c) supports that the tracking error increases immediately after every impact.

Fig. 4 shows the simulation results of dynamic walking where $f_c = 3.0$ [Hz]. In this case, as discussed in the next section, the dynamics of the wobbling mass has a strong influence on the CRW and the walking pattern is entrained to the wobbling motion. This is confirmed by seeing the convergence of the instant of discontinuous change in $\dot{L}_c$. It is also confirmed that $\dot{L}_c$ discontinuously increases immediately after every impact as shown in the previous section.

Fig. 5 shows the time evolutions of the angular positions where (a) $f_c = 1.85$ [Hz], (b) $f_c = 1.90$ [Hz], and (c) $f_c = 1.95$ [Hz]. Fig. 5 (b) shows that the walker cannot overcome the potential barrier at mid-stance and falls backward. Destabilization of the generated gait is mainly caused by the failure to overcome the potential barrier. This is analyzed in more detail later. As the simulation results suggest, the limit cycle stability is highly sensitive to the initial conditions.

Table 1 Parameter settings for simulation model

$m_1(= m_2)$	Mass of each RW	1.0	kg
m_3	Mass of body frame	1.0	kg
m_c	Wobbling mass	1.0	kg
$L(= L_1 = L_2)$	Leg length	0.15	m
L_3	Half length of body frame	0.20	m
ϕ	Slope angle	0.07	rad
A_m	Amplitude of pumping motion	0.03	m
K_D	Derivative gain	100	
K_P	Proportional gain	2500	

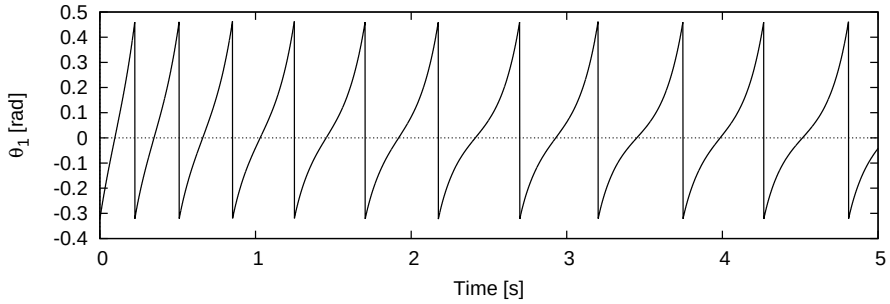

(a) θ_1 [rad]

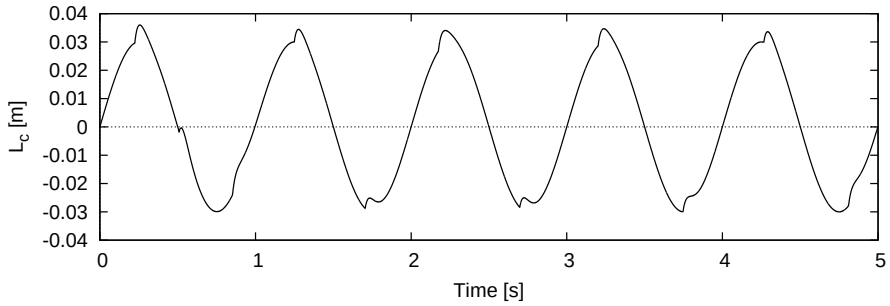

(b) L_c [m]

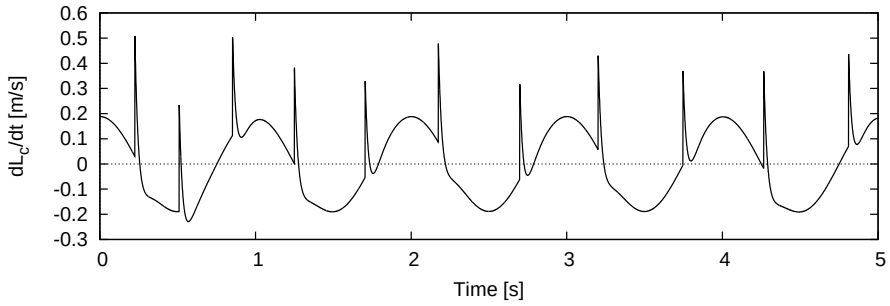

(c) $\dot{L}_c$ [m/s]

Fig. 3 Simulation results where $f_c = 1.0$ [Hz]

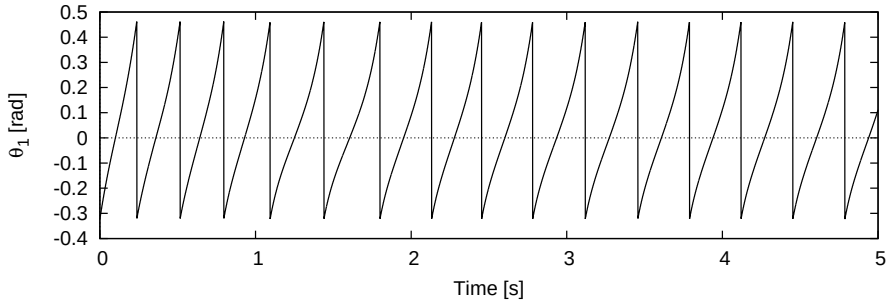

(a) θ_1 [rad]

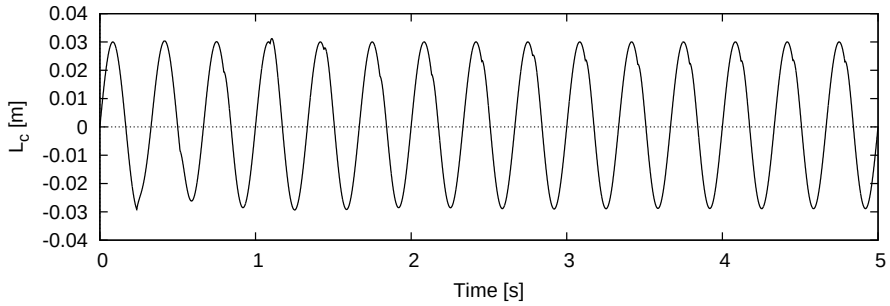

(b) L_c [m]

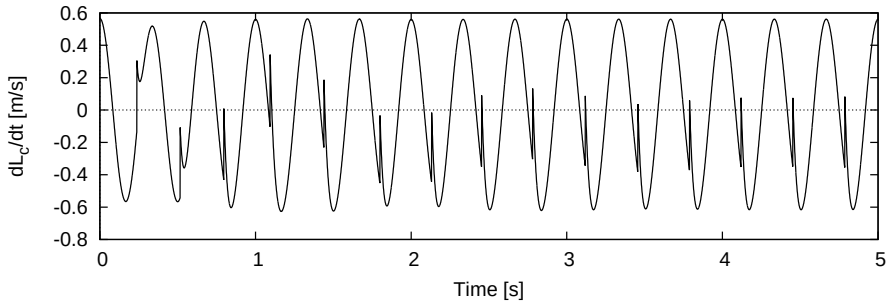

(c) $\dot{L}_c$ [m/s]

Fig. 4 Simulation results where $f_c = 3.0$ [Hz]

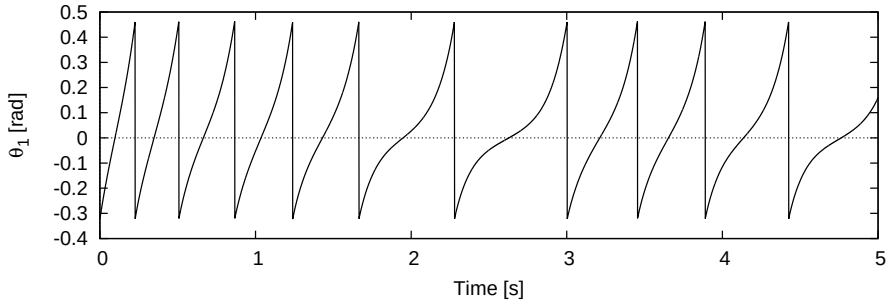

(a) $f_c = 1.85$ [Hz]

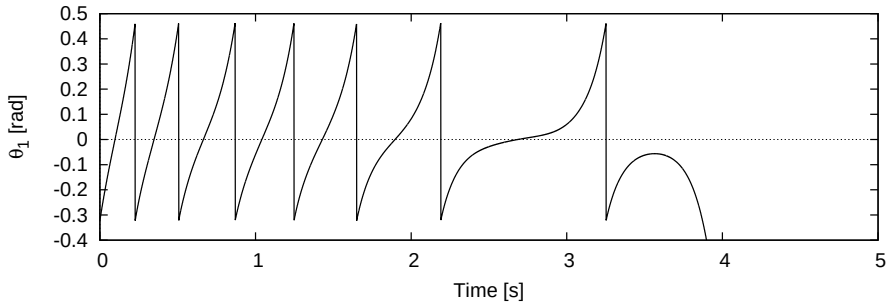

(b) $f_c = 1.90$ [Hz]

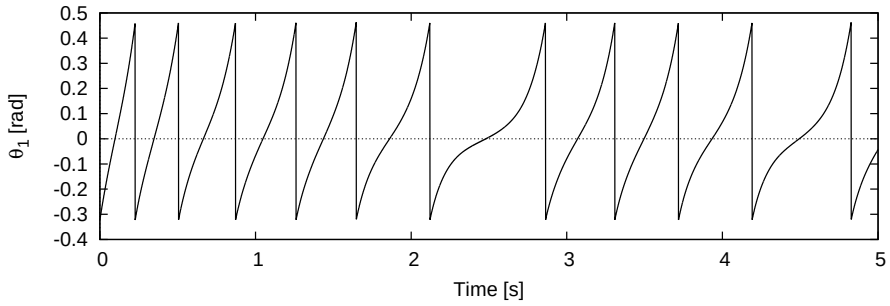

(c) $f_c = 1.95$ [Hz]

Fig. 5 Simulation results for three consecutive values of f_c [Hz]

4 Gait analysis

4.1 Gait descriptors

We consider two criteria for understanding the gait properties; one is the frequency of walking gait and the other is the phase difference between the CRW and the wobbling mass. Let T [s] be the step period. The frequency of the CRW is then determined as the reciprocal of the step period, $f_w = 1/T$ [Hz]. This is in other words the cadence of walking motion. The phase difference, ψ

[rad], is also defined as

$$\psi := \frac{2\pi(t_c - t_w)}{T}.$$

Here, t_w [s] is the instant, at which the perpendicular distance between the CoM position of the CRW body and the floor is maximized. t_c [s] is the instant, at which L_c reaches minimum or the relative position of the wobbling mass from the body frame reaches to the topmost height. A negative phase implies that a movement of the wobbling mass is advanced to that of the CRW, whereas a positive phase indicates a reversed relationship.

4.2 Effect of wobbling frequency

We studied dependence of dynamic walking on the slope angle ϕ [rad] for four values of m_c [kg] according to the following procedure. In the case that λ_2 is not always positive, we decided that a stable gait could not be successfully generated.

(A1) Set the slope angle and the desired wobble frequency to $\phi = 0.07$ [rad] and $f_c = 0$ [Hz].
(A2) Set the initial conditions to the values of Eq. (27), and start dynamic walking.
(A3) After 100 [s] from the start, save the gait descriptors for 20 steps.
(A4) Increase f_c by 0.05 [Hz] and return to (A2).
(A5) Repeat from (A2) to (A4) until $f_c = 5.0$ [Hz].

Figs. 6 and 7 respectively show dependence of the frequency of the CRW, f_w [Hz], and the phase difference, ψ [rad], on the frequency of the wobbling mass, f_c [Hz]. By focusing mainly on Fig. 6 (c), a typical transition from desynchronization to synchronization between the CRW and the wobbling mass can be observed [14]. For a small frequency of $f_c < 1.0$ [Hz], the CRW is only weakly influenced by the wobbling mass and it oscillates with its own natural frequency of around 1.87 [Hz]. As f_c is increased from 1.0 [Hz], the motion of the CRW is more strongly modulated by the up-and-down movement of the wobbling mass and f_w takes different values in every walking step. Here, the dense plots of f_w represent a sign of quasi-periodic motion. The averaged frequency of f_w, however, remains in a similar range to the natural frequency. As f_c becomes close to 1.75 [Hz], f_w shows a periodic motion, whose value coincides with f_c (f_w grows on a diagonal line of $f_w = f_c$). This indicates that the motion of the CRW is entrained to the up-and-down movement of the wobbling mass [14].

As seen in a range of small f_c in Fig. 6 (a)-(d), we can see that the natural frequency of the CRW is slightly increased as the wobbling mass is increased. That is, the moving speed in passive dynamic walking monotonically increases as m_c increases. This is because kinetic energy loss at impact decreases with the increase of m_c as shown in the previous section.

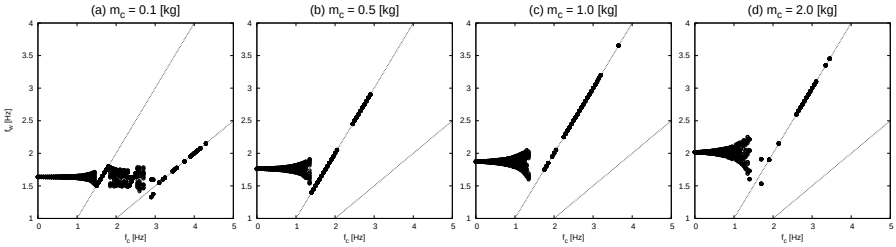

Fig. 6 f_w for four values of m_c with respect to f_c

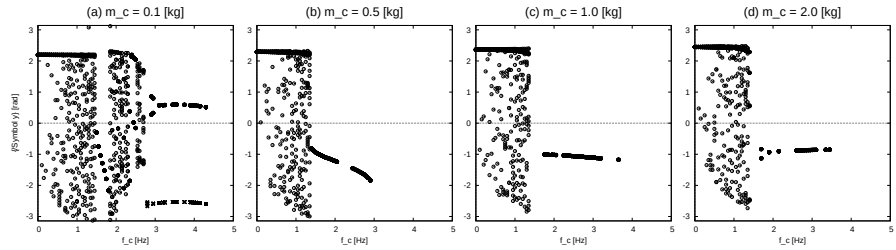

Fig. 7 ψ for four values of m_c with respect to f_c

As indicated by positive phase difference, ψ, in Fig. 7, initially, the oscillatory phase of the wobbling mass is delayed from that of the CRW (*i.e.*, anti-phase synchronization), since f_c is smaller than the natural frequency of the CRW. As f_c grows large, the two frequencies become similar to each other and the in-phase synchronization takes place. As f_c grows larger than the natural frequency of the CRW, the phase of the wobbling mass is advanced to that of the CRW (*i.e.*, anti-phase synchronization) as confirmed by negative phase difference in Fig. 7. This represents a desired state of walking, because (1) trajectory of the CoM is flattened by the anti-phase synchronization between the CRW and the wobbling mass, which was proved optimal for walking in [10], and (2) the frequency of the CRW is accelerated by the wobbling mass.

It should be noted that for a small wobbling mass ($m_c = 0.1$ [kg]), the 1:1 entrainment (*i.e.*, $f_c = f_w$) is broken around $f_c = 1.8$ [Hz], giving rise to regime of desynchronization as shown in Fig. 7 (a). This implies that the small wobbling mass cannot entrain the CRW so strongly compared to larger masses. For $f_c > 3.0$ [Hz], however, the CRW is entrained to a half value of the wobbling frequency ($f_w = f_c/2$). As shown in Fig. 8, during one walking step, the wobbling mass moves up-and-down twice, giving rise to two sorts of phase differences with respect to t_{c1} and t_{c2} that appear before and after t_w (indicated by "◯" and "×" in Fig. 7 (a)). This represents 1:2 entrainment widely observed in coupled nonlinear oscillators [14]. The maximum walking speed is not so high compared with those at the low frequency. This is because the effect of indirect excitation in this case is small due to the light weight.

Fig. 9 plots the cause of unsteady gait for four values of m_c. Here, "×" represents the case of falling backward whereas "▲" represents that of negative

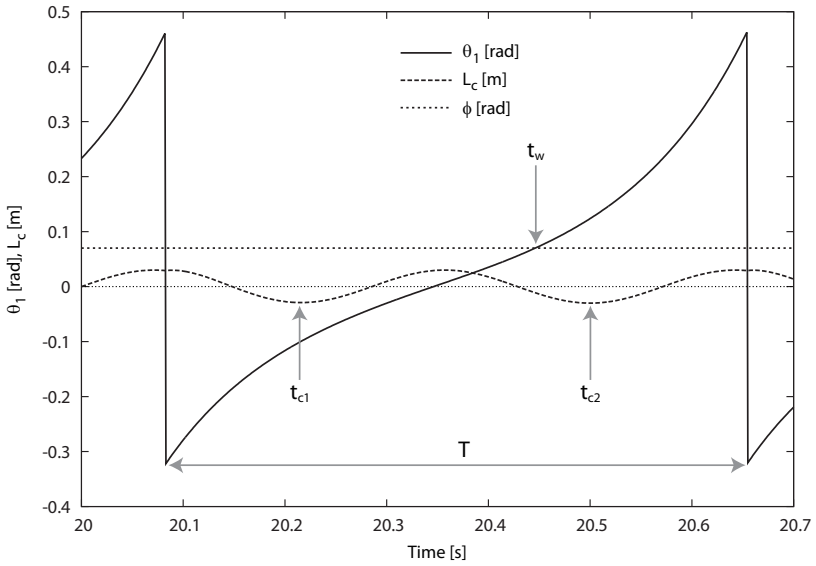

Fig. 8 Steady trajectories of θ_1 and L_c for one step where $\phi = 0.07$ [rad] and $f_c = 3.5$ [Hz]

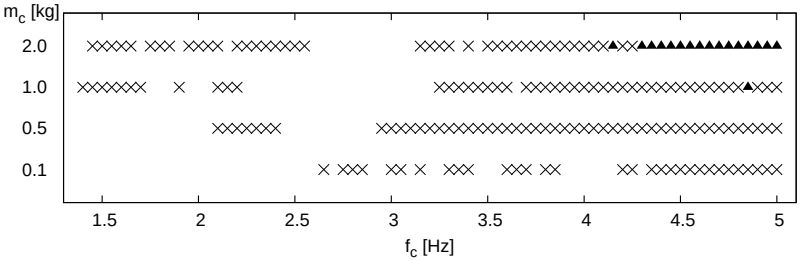

Fig. 9 Cause for unsteady gait

λ_2. We can see that most of the unsteady gaits are caused by the failure to overcome the potential barrier.

4.3 Effect of slope

We also investigated how the generated gait properties change with respect to the slope and performed numerical simulations according to the following procedure.

(B1) Set the slope angle and the desired wobble frequency to $\phi = 0.06$ [rad] and $f_c = 3.5$ [Hz].
(B2) Set the initial conditions to the values of Eq. (27), and start dynamic walking.
(B3) After 100 [s] from the start, save the gait descriptors for 20 steps.

(B4) Increase ϕ by 0.001 [rad] and return to (B2).
(B5) Repeat from (B2) to (B4) until $\phi = 0.18$ [rad].

Figs. 10 and 11 respectively show dependence of the frequency of the CRW, f_w [Hz], and the phase difference, ψ [rad], on the slope, ϕ [rad].

As in Figs. 6 and 7, transitions from desynchronization to synchronization between the CRW and the wobbling mass are discernible. In this case, increase in the slope angle ϕ monotonically increases the walking frequency f_w of the CRW. As the walking frequency f_w crosses the modulation frequency f_c of the wobbling mass, f_w is locked to f_c, showing a flat regime of $f_w = f_c$. Here, the CRW is entrained to the dynamics of the wobbling mass. The range of entrainment is increased as the size of the wobbling mass is increased from (a) to (d). This indicates that the wobbling mass entrains the CRW more strongly as the mass size is increased.

For a small mass shown in (a), 1:2 entrainment appears in the range of a small slope ($\phi \leq 0.073$ [rad]). The generated gait converges to a periodic motion with $f_w = f_c/2 = 1.75$ [Hz]. As the slope angle is increased from this range, the 1:2 entrainment is broken at $\phi = 0.073$ [rad] and 1:1 entrainment appears for $0.097 \leq \phi \leq 0.107$ [rad].

Fig. 11 shows that the phase difference ψ takes different values in every walking step when the CRW and the wobbling mass are not synchronized with each other. When they are synchronized, on the other hand, the phase difference is locked to a constant value. Here, the phase difference increases monotonically as the natural frequency of the CRW is increased by the inclined slope angle ϕ. When the natural frequency of the CRW exceeds f_c, the CRW

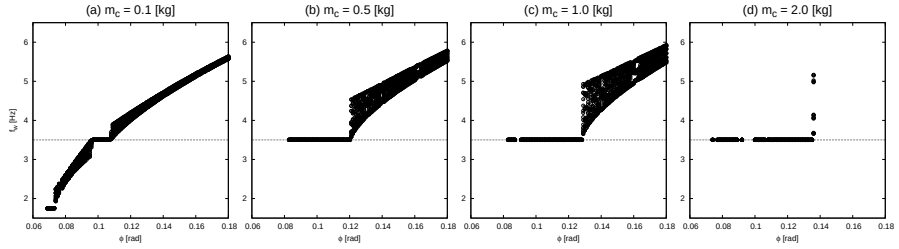

Fig. 10 f_w for four values of m_c with respect to f_c

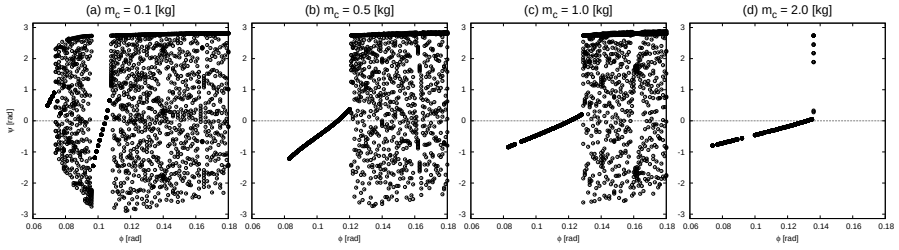

Fig. 11 ψ for four values of m_c with respect to f_c

becomes phase-advanced from the wobbling mass, resulting in a positive phase difference ($\psi > 0$). This sort of phase relationship is commonly observed in forced self-sustained oscillators [14].

5 Experimental case study

5.1 Specifications of experimental machine

Fig. 12 shows an overview of our prototype CRW machine with the drive unit and the wobbling mass. The wobbling mass consists of three weight plates whose mass is 450 [g], and the whole moving weight is 1508 [g]. It moves up-and-down along the guide rail according to the piston crank mechanism driven by a maxon DC motor. It is also connected to a constant force spring from above to reduce the load of the DC motor.

The total mass of the drive unit is 3070 [g]. Other parameters are also listed in Table 2. The fore and rear RWs are connected by a rigid rod so that they move in a complete synchronization.

The motor driver controls the DC motor in speed-control mode so that it rotates at a constant rotating speed under load. The generated up-and-down motion of the wobbling mass represents an almost sinusoidal waveform. The amplitude of the motion can be adjusted by changing the mounting position to the crankshaft. In this paper, we chose the amplitude as $A_m = 35$ [mm].

5.2 Experimental results

We performed walking experiments on an inclined treadmill where the slope angle was set to 3.9 [deg]. We changed the frequency of the wobbling mass, f_c [Hz], from zero to 3.0 [Hz] and recorded the steady treadmill speeds five times for each frequency to compute average walking speeds.

Fig. 13 plots the experimental results of the walking speed with respect to the desired wobble frequency. We can see that the generated walking speed shows only a little change from $f_c = 0$ to 1.5 [Hz], whereas it begins to monotonically increase in the range of $f_c \geq 2.0$ [Hz]. With the increase of f_c, frequency entrainment occurs and indirectly-excited walking motion is generated. Note that the driving system has a little back-drivability and this is the largest difference between experiments and numerical simulations. This also causes the

Table 2 Physical parameters of experimental CRW machine

Total mass of drive unit	3070	g
Wobbling mass	1508	g
One weight plate	450	g
One rimless wheel	800	g
Body frame	1300	g
Leg length (radius)	150	mm

difference of the impact dynamics. The experimental result agrees well with the numerical analysis in spite of the high rigidity of the driving system.

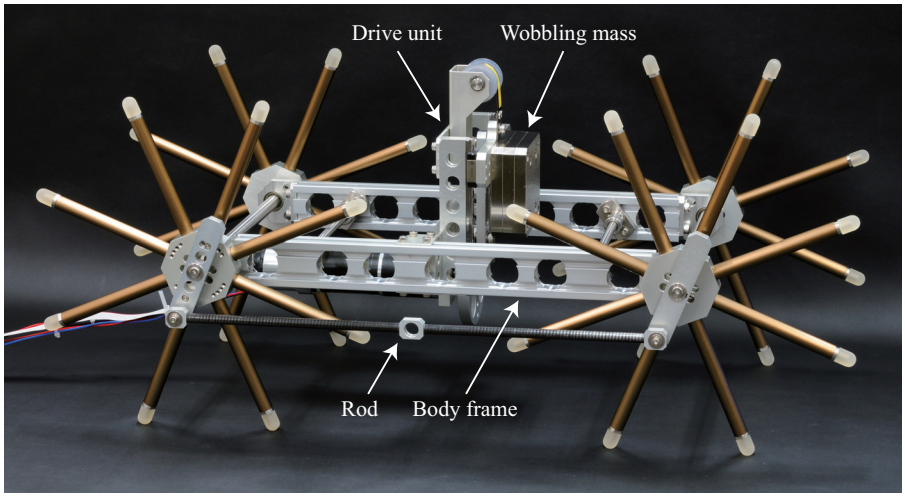

(a) Side view

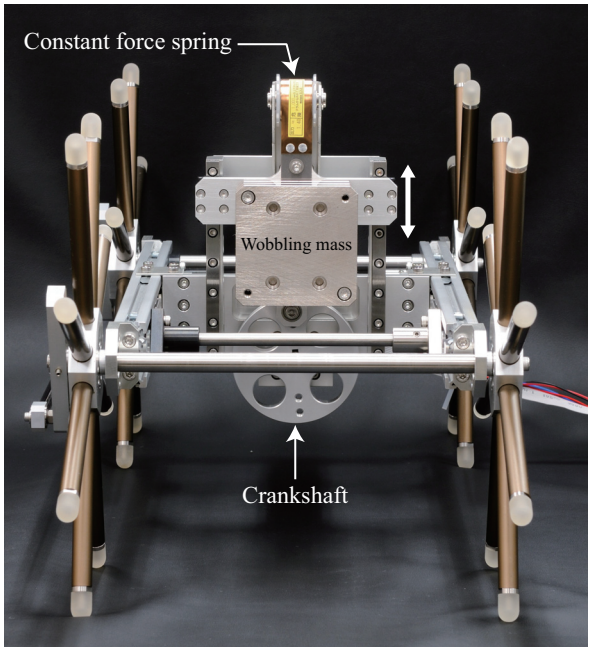

(b) Front view

Fig. 12 Overview of experimental CRW with active wobbling mass

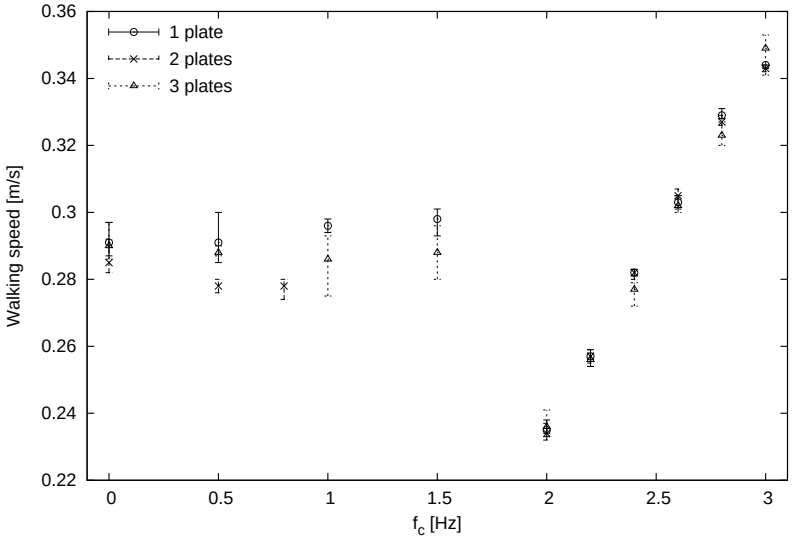

Fig. 13 Experimental result of controlled walking speed with respect to f_c

6 Conclusion and future work

In this paper, we investigated the effect of indirect excitation control of the active wobbling mass moving up-and-down in the body frame. Through numerical simulations and experiments, we clarified that frequency entrainment occurs and speeding-up is accordingly achieved at the high frequencies of the wobbling mass. One of the strong advantages of our indirectly-excited motion generation is the easiness of its implementation, which may enlarge its wide applicability. For instance, we can easily generate or enhance performance of dynamic walkers by simply attaching the drive unit afterward.

Currently we are investigating the potentiality of level dynamic walking using the principle of indirect excitation. Unlike the continuous control of the active wobbling mass studied in this paper, phase resetting would be necessary to successfully restore mechanical energy lost by collision. The use of a wobbling mass with multi-DOF that can allow translational and rotational movements is also an interesting subject for study. The ultimate objective of our study is to develop a design method for passive/active wobbling masses that optimize the gait efficiencies of general legged locomotion robots.

Acknowledgements The authors would like to thank ONO-DENKI CO., LTD. for many helpful suggestions and technical supports in development of the prototype walking machine. They also wish to thank the members of JAIST Asano Laboratory for supporting the walking experiments.

Appendix A

The details of the matrix $\boldsymbol{M}(\boldsymbol{q})$ and the vector $\boldsymbol{h}\left(\boldsymbol{q}, \dot{\boldsymbol{q}}\right)$ in Eq. (1) are as follows.

$$\boldsymbol{M}(\boldsymbol{q}) = \begin{bmatrix} \boldsymbol{M}_1(\boldsymbol{q}) & \boldsymbol{0}_{3\times3} & \boldsymbol{0}_{3\times4} \\ \boldsymbol{0}_{3\times3} & \boldsymbol{M}_2(\boldsymbol{q}) & \boldsymbol{0}_{3\times4} \\ \boldsymbol{0}_{4\times3} & \boldsymbol{0}_{4\times3} & \boldsymbol{M}_3(\boldsymbol{q}) \end{bmatrix} \tag{28}$$

$$\boldsymbol{M}_1(\boldsymbol{q}) = \begin{bmatrix} m_1 & 0 & m_1 L_1 \cos\theta_1 \\ 0 & m_1 & -m_1 L_1 \sin\theta_1 \\ m_1 L_1 \cos\theta_1 & -m_1 L_1 \sin\theta_1 & m_1 L_1^2 + I_1 \end{bmatrix} \tag{29}$$

$$\boldsymbol{M}_2(\boldsymbol{q}) = \begin{bmatrix} m_2 & 0 & m_2 L_2 \cos\theta_2 \\ 0 & m_2 & -m_2 L_2 \sin\theta_2 \\ m_2 L_2 \cos\theta_2 & -m_2 L_2 \sin\theta_2 & m_2 L_2^2 + I_2 \end{bmatrix} \tag{30}$$

$$\boldsymbol{M}_3(\boldsymbol{q}) = \begin{bmatrix} m_3 + m_c & 0 & -m_c L_c \cos\theta_3 & -m_c \sin\theta_3 \\ 0 & m_3 + m_c & m_c L_c \sin\theta_3 & -m_c \cos\theta_3 \\ -m_c L_c \cos\theta_3 & m_c L_c \sin\theta_3 & m_c L_c^2 & 0 \\ -m_c \sin\theta_1 & -m_c \cos\theta_3 & 0 & m_c \end{bmatrix} \tag{31}$$

$$\boldsymbol{h}\left(\boldsymbol{q}, \dot{\boldsymbol{q}}\right) = \begin{bmatrix} \boldsymbol{h}_1\left(\boldsymbol{q}, \dot{\boldsymbol{q}}\right) \\ \boldsymbol{h}_2\left(\boldsymbol{q}, \dot{\boldsymbol{q}}\right) \\ \boldsymbol{h}_3\left(\boldsymbol{q}, \dot{\boldsymbol{q}}\right) \end{bmatrix} \tag{32}$$

$$\boldsymbol{h}_1\left(\boldsymbol{q}, \dot{\boldsymbol{q}}\right) = \begin{bmatrix} -m_1 L_1 \dot{\theta}_1^2 \sin\theta_1 \\ m_1\left(g - L_1 \dot{\theta}_1^2 \cos\theta_1\right) \\ -m_1 g L_1 \sin\theta_1 \end{bmatrix} \tag{33}$$

$$\boldsymbol{h}_2\left(\boldsymbol{q}, \dot{\boldsymbol{q}}\right) = \begin{bmatrix} -m_2 L_2 \dot{\theta}_2^2 \sin\theta_2 \\ m_2\left(g - L_2 \dot{\theta}_2^2 \cos\theta_2\right) \\ -m_2 g L_2 \sin\theta_2 \end{bmatrix} \tag{34}$$

$$\boldsymbol{h}_3\left(\boldsymbol{q}, \dot{\boldsymbol{q}}\right) = \begin{bmatrix} m_c \dot{\theta}_3^2\left(L_c \dot{\theta}_3 \sin\theta_3 - 2\dot{L}_c \cos\theta_3\right) \\ (m_3 + m_c) g + m_c \dot{\theta}_3\left(L_c \dot{\theta}_3 \cos\theta_3 + 2\dot{L}_c \sin\theta_3\right) \\ m_c L_c\left(g \sin\theta_3 + 2\dot{L}_c \dot{\theta}_3\right) \\ -m_c\left(g \cos\theta_3 + L_c \dot{\theta}_3^2\right) \end{bmatrix} \tag{35}$$

Note that we added inertia moments for the fore and rear RWs, I_1 and I_2, as indicated in Eqs. (29) and (30). This is necessary to calculate $\boldsymbol{M}(\boldsymbol{q})^{-1}$ in the derivations of $\boldsymbol{\lambda}$ and $\ddot{\boldsymbol{q}}$. After that, we finally took the limits of $I_1 \to 0$ and $I_2 \to 0$ for deriving Eq. (9).

References

1. T. McGeer, "Passive dynamic walking," *Int. J. of Robotics Research*, Vol. 9, No. 2, pp. 62–82, 1990.

2. C. Chevallereau, G. Abba, Y. Aoustin, F. Plestan, E. R. Westervelt, C. Canudas-de-Wit and J. W. Grizzle, "RABBIT: A Testbed for advanced control theory," *IEEE Control Systems Magazine*, Vol. 23, No. 5, pp. 57–79, 2003.
3. R. Tedrake, T. W. Zhang, M. Fong and H. S. Seung, "Actuating a simple 3D passive dynamic walker," *Proc. of the IEEE Int. Conf. on Robotics and Automation*, pp. 4656–4661, 2004.
4. C. D. Remy, K. Buffinton and R. Siegwart, "Stability analysis of passive dynamic walking of quadrupeds," *Int. J. of Robotics Research*, Vol. 29, No. 9, pp. 1173–1185, 2010.
5. Y. Sugimoto, H. Yoshioka and K. Osuka: "Realization and motion analysis of multi-legged passive dynamic walking," *Proc. of the SICE Annual Conference*, pp. 2790–2793, 2010.
6. M. J. Coleman, A. Chatterjee and A. Ruina, "Motions of a rimless spoked wheel: a simple three-dimensional system with impacts," *Dynamics and Stability of Systems*, Vol. 12, Iss. 3, pp. 139–159, 1997.
7. F. Asano, "Stability principle underlying passive dynamic walking of rimless wheel," *Proc. of the IEEE Int. Conf. on Control Applications*, pp. 1039–1044, 2012.
8. F. Asano, "Efficiency and optimality of two-period limit cycle walking," *Advanced Robotics*, Vol. 26, No. 1-2, pp. 155–176, Jan. 2012.
9. R. Inoue, F. Asano, D. Tanaka and I. Tokuda, "Passive dynamic walking of combined rimless wheel and its speeding-up by adjustment of phase difference," *Proc. of the IEEE/RSJ Int. Conf. on Intelligent Robots and Systems*, pp. 2747–2752, 2011.
10. D. Tanaka, F. Asano and I. Tokuda, "Gait analysis and efficiency improvement of passive dynamic walking of combined rimless wheel with wobbling mass," *Proc. of the IEEE/RSJ Int. Conf. on Intelligent Robots and Systems*, pp. 151–156, 2012.
11. J. Ackerman and J. Seipel, "Energetics of bio-inspired legged robot locomotion with elastically-suspended loads," *Proc. of the IEEE/RSJ Int. Conf. on Intelligent Robots and Systems*, pp. 203–208, 2011.
12. L. C. Rome, L. Flynn, E. M. Goldman and T. D. Yoo, "Generating electricity while walking with loads," *Science*, Vol. 309, No. 5741, pp. 1725–1728, 2005.
13. L. C. Rome, L. Flynn and T. D. Yoo, "Biomechanics: Rubber bands reduce the cost of carrying loads," *Nature*, Vol. 444, No. 7122, pp. 1023–1024, 2006.
14. A. Pikovsky, M. Rosenblum, and J. Kurths, *Synchronization: A Universal Concept in Nonlinear Sciences*, Cambridge University Press, Cambridge, 2003.